Molecular Tailoring Approach for Simulation of Electrostatic Properties

Shridhar R. Gadre,* Rajendra N. Shirsat, and Ajay C. Limaye

Department of Chemistry, University of Poona, Pune 411007, India

*Received: February 23, 1994**

A method for synthesizing ab initio molecular electrostatic potential (MESP) and field (MEF) by "stitching" together suitably tailored smaller fragments is presented. The procedure is assessed for its ability to mimic the ab initio MESP and its topography for the model cases of zeolite silicon pentamer ($Si_5O_{16}H_{12}$) and decamer ($Si_{10}O_{10}H_{20}$) and has been found fairly reliable. A further application to di- and tripeptides is shown to simulate well the ab initio MESP and MEF with the respective MESP minima reproduced to within 1% or less. This reliability, coupled with bypassing of the SCF computation of the tailored molecule, makes the approach an attractive one for exploring one-electron properties of large molecular systems.

Introduction

A practising chemist is always interested in developing simple theoretical models for the study of electronic properties and reactivities of molecules. The molecular electrostatic potential (MESP) has been found[1-5] to be an invaluable tool for this purpose and is widely applied for investigating catalysts, biomolecules, drugs, high-energy molecules, etc. The MESP, $V(\mathbf{r})$, is defined as

$$V(\mathbf{r}) = \sum_{A=1}^{N} \frac{Z_A}{|\mathbf{r} - \mathbf{R}_A|} - \int \frac{\rho(\mathbf{r}')}{|\mathbf{r}' - \mathbf{r}|} d^3r' \qquad (1)$$

where Z_A is the charge of a nucleus located at $\mathbf{R}_A$ and $\rho(\mathbf{r})$ is the molecular electron density. The MESP is thus a sum of two parts, the positive nuclear contribution and the negative electronic one: the first and the second terms in eq 1, respectively. Due to this, the MESP is capable of exhibiting rich topographical features.[6-8] The negative-valued MESP minima have been widely employed in the literature for locating probable sites of electrophilic attack[1,2] as well as for correlating[9,10] the proton affinities of various sites in molecular clusters. On the other hand, MESP textured on a surface has been employed for exploring nucleophilic attack. Semiempirical procedures can also be employed for computing MESP and the molecular electrostatic field (MEF, i.e., $-\nabla V$). However, quantitatively more reliable results are obtained via the ab initio LCAO-MO approaches. Within the MO framework, the electronic part (second term in eq 1) of the MESP is written as

$$V_{elec}(\mathbf{r}) = -\sum_{i,j} P_{ij} \int \frac{\phi_i(\mathbf{r}')\, \phi_j^*(\mathbf{r}')}{|\mathbf{r}' - \mathbf{r}|} d^3r' \qquad (2)$$

Here, indices i and j run over the total number of atomic orbitals (AOs) or contractions denoted by ϕ_i. Though the computation of ab initio MESP over a large number of grid points is a CPU-intensive task, efficient algorithms for this purpose have recently[8] been devised and tested. In these algorithms, it has been explicitly demonstrated that this calculation, originally $O(N^2)$, in complexity gets reduced to $O(N)$, since an AO can effectively yield contributions mainly with a few neighbouring ones. This is essentially due to the $1/|\mathbf{r} - \mathbf{r}'|$ weighting factor in the definition of $V(\mathbf{r})$ (cf eq 1) as well as the exponential decay of the overlap of orbitals. Thus, the main hurdle in obtaining the ab initio MO-based MESP still remains to be the $O(N^3$ to $N^4)$ dependence of the SCF procedure. The implementation of ab initio SCF procedure *for large molecules* is still a prohibitive task, especially on workstation-range machines. Studies based on bond fragments for obtaining electrostatic fields of large molecules have been attempted[11] earlier to overcome this difficulty. The approach here is to employ transferable localized molecular orbitals mostly within semiempirical procedures. Quantitative comparison of fine features such as the topography of MESP are not attempted within such investigations. A method for implementing ab initio calculation on large molecules has been developed and extensively tested by Christoffersen[12] and co-workers. The goals for this method as stated by Christoffersen[12] in as early as 1972 are to apply ab initio procedure conforming to chemical intuition, to systems with around 200 electrons and 75 nuclei. It is desirable[12] that such a method should yield all properties with about equal and acceptable accuracy. However, the actual applications reported by Christoffersen were mostly limited to floating spherical Gaussians, partly due to the limitations of available hardware in the 1970s and early 1980s. A novel approach recently developed by Lee and Friesner[13] which exclusively deals with extraction of point charges for large molecules has come to our attention after the first version of the present MS was completed. A part of the methodology termed by them as fragment density approach bears some resemblance to the present molecular tailoring method. The main motive of our work is, on the other hand, to explore the electrostatic properties of "synthesized" molecules as applied to a wide variety of chemically interesting systems. A detailed critical comparison of the present method with that by Lee and Friesner[13] will be presented in the following sections.

Fragmentation Approach

The fragments approach is centered around the fact that the electronic contributions vide eq 2 are a local phenomenon in large molecular systems. These contributions to the electrostatic potential and field over a region in space are mostly due to the "nearer" interacting portion of the molecular system. Hence, to simulate the electrostatics in space, one can either implicitly or explicitly ignore the electronic contributions due to interactions between the farthest portions of the molecule. In the conventional method, one carries out an ab initio SCF calculation for the whole system and then ignores the insignificant contributions while computing MESP and MEF. This conventional method is known to have practical restrictions on the size of the molecule for its ab initio SCF study (in terms of number of basis functions, typically ~1000 on supercomputers and ~300 on workstations when no symmetry features are exploited). Moreover, the time required to obtain the ab initio wave function is prohibitively large. In light of these limitations, a new methodology is proposed for accommodating very large systems for molecular electrostatics

* Abstract published in *Advance ACS Abstracts*, August 1, 1994.

0022-3654/94/2098-9165$04.50/0

investigations, by implementing SCF of only suitably formed smaller fragments.

In this "tailoring" method, one breaks the molecule into smaller overlapping fragments as tailors cut the fabric. The ab initio SCF calculations are then effected for each of these fragments to get their wave functions. The resulting density matrices are suitably "stitched" to form the "synthesized" density matrix for the whole molecular system which is hopefully a good approximation to its SCF counterpart. If the fragments are mutually exclusive (i.e., there is no overlap), then the interfragment interaction will be taken to be zero. This interaction is nearly zero between distant atoms, but for nearer ones it is certainly not negligible. To get a good "synthesized" density matrix, it is thus imperative that the fragmentation and its overlapping are done with due caution. It may not be prudent to break double/triple bonds, small rings (e.g., benzene ring), small groups (e.g., methyl, nitro, hydroxyl groups, etc.) and pendent atoms. One must take care that a fragment must have a connected graph. Also, the fragments should be large enough to correctly simulate the effects of the interior atoms of that fragment. While the fragments are stitched, density matrix elements should be taken from that fragment in which the corresponding interactions are well-simulated. This method is not, of course, meant to be applied to the small molecular systems: such an approach may not be worthwhile in that situation. The present procedure as well as that by Lee and Friesner[13] ignore the interfragment contribution to MESP. We invoke no assumptions for intrafragment elements. However, Lee and Friesner[13] make intrafragment *P2zero* and *P3zero* approximations (neglect of more than second- and third-neighbor interactions, respectively); further, they make a choice of uniform scale factor which is obtained from a formula (eq 11 in ref 13). We on the other hand, check whether trace of the product of density matrix (**P**) and the corresponding overlap matrix (**S**) equals the number of electrons and scale **P** accordingly. Further, we compute the norm of (**PSP** − **2P**) for providing a check on the idempotency of **P**. A general FORTRAN code has been developed and tested for obtaining synthesized **P** from the corresponding fragment **P**'s and is available from the authors upon request.

The above scheme of stitching density matrices has been tested for a number of systems exhibiting a variety of connectivities. The electrostatic potential which exhibits rich topographical features, is used as a yardstick for appraising the efficacy of the present approach. The test cases studied are silicon pentamer ($Si_5O_{16}H_{12}$), decamer[14] with hydrogen-terminated silicons ($Si_{10}O_{10}H_{20}$), and decamer ($Si_{10}O_{30}H_{20}$; the latter three are a part of ZSM-5 zeolite). Finally, applications to interacting amino acids, with di- and tripeptides as examples, are presented. The test cases chosen here are such that they exhibit a variety of structural features such as ringed and branched structures.

In the case of silicon pentamer, appropriate trimers (with terminal oxygens saturated with hydrogens) are treated as the overlapping fragments (as shown in Figure 1a). The central silicon ($Si^{\dagger}$) and the attached oxygens (O^a, O^b, O^c, and O^d) form the overlapping part. The molecule being reasonably small here, it is broken into only two fragments. The synthesis of **P** is schematically presented in Figure 1b. The contributions taken from fragment 1 are (1) self- and cross-interactions of $(SiO_3)^a$, $(SiO_3)^c$, $Si^{\dagger}$, O^a, and O^c; (2) cross-interactions of O^b and O^d with $(SiO_3)^a$, $(SiO_3)^c$, and $Si^{\dagger}$. The contributions taken from fragment 2 are (3) self- and cross-interactions of O^b and O^d; (4) self- and cross-interactions of $(SiO_3)^b$ and $(SiO_3)^d$; (5) cross-interactions of $Si^{\dagger}$, O^a, O^b, O^c, and O^d with $(SiO_3)^b$ and $(SiO_3)^d$.

In the decamer cases ($Si_{10}O_{10}H_{20}$ and $Si_{10}O_{30}H_{20}$), the molecules are fragmented into three overlapping regions (with terminal oxygens suitably protonated), viz., one pentamer and two tetramers as shown in Figure 2. Each of the three overlapping regions in the ring is an O–Si–O part. The decamer systems

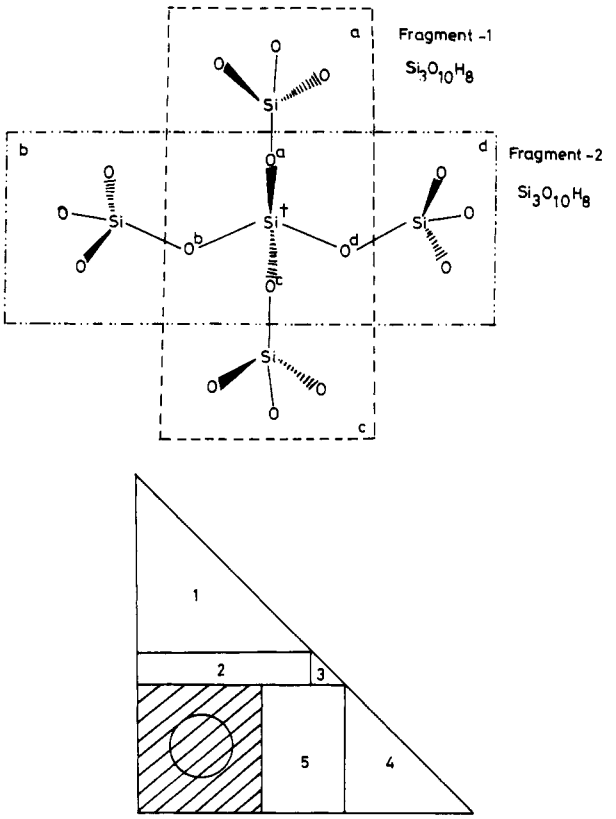

Figure 1. (a, top) Fragmentation scheme for $Si_5O_{16}H_{12}$. Hydrogens not shown in schematic. (b, bottom) The schematic tailored density matrix for $Si_5O_{16}H_{12}$.

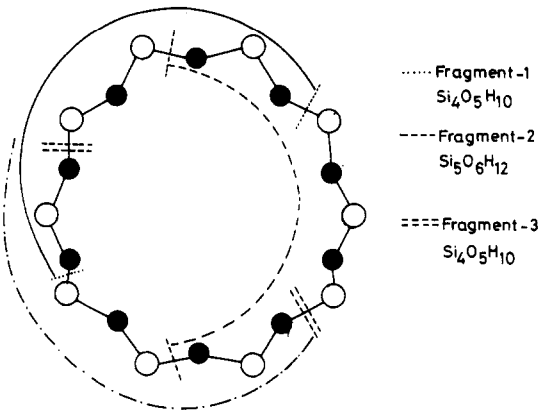

Figure 2. Fragmentation scheme for decamer ring: $Si_{10}O_{10}H_{20}$. Terminal hydrogens not shown in the schematic. The dark and white circles represent oxygen and silicon atoms, respectively.

being rings, the assembled density matrices contain a belt of zeros separating two significant regions.

The usefulness of the fragmentation approach is also assessed for a model di- and tripeptide which are prototypes of polar molecules. The dipeptide chain (phe-his) consists of phenylalanine ($C_9NO_2H_{12}$) connected to histidine ($C_6N_3O_2H_9$) through a peptide linkage forming the backbone of the molecule. The tripeptide chain (phe-his-try) consists of phenylalanine, histidine, and tryptophan ($C_{11}N_2O_2H_{12}$). The synthesized **P** for the dipeptide chain is obtained from the two density matrices pertaining to the two fragments of phenylalanine and histidine, respectively, with suitable overlaps. The tripeptide chain is fragmented into four parts consisting of phenylalanine, histidine, tryptophan, and the backbone with suitable overlaps.

The features of MESP and its topography as well as MEF obtained for the above test cases are discussed in the following section.

TABLE 1: Statistical Error Analysis for Tailored Density Matrices and the Total SCF Time (seconds) of Fragments and Full Calculation, Respectively (au Wherever Appropriate)

molecule and basis set	no. of contractions	deviations[a]			total SCF time[b]	
		std	av	max	syn[c]	actual
$Si_5O_{16}H_{12}$ (STO-3G)	137	3.3e–3	1.1e–3	8.5e–2	4340	39 670
$Si_{10}O_{10}H_{20}$ (STO-3G)	160	2.2e–3	7.2e–4	4.5e–2	4539	40 100

[a] Standard deviation = $\{(1/N)\sum_{i=1}^{N}(D_{act}^{(i)} - D_{syn}^{(i)})^2\}^{1/2}$. Average deviation = $(1/N)\sum_{i=1}^{n}|D_{act}^{(i)} - D_{syn}^{(i)}|$; N = number of entries. D_{act} and D_{syn} stand for the actual and synthesized density matrices, respectively. [b] SCF carried out on 16-node PARAM in direct mode with integral and SCF cutoffs of 10^{-10} and 10^{-7} au, respectively. [c] SCF timings for all the fragments are added to get the total time.

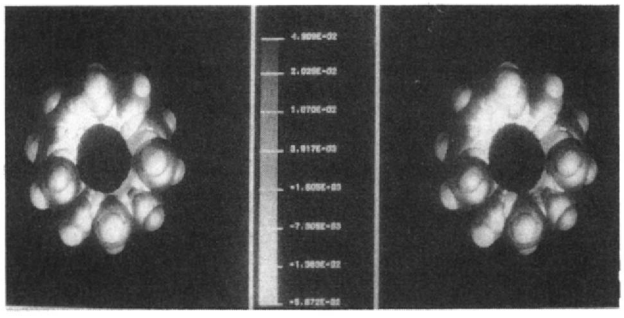

Figure 3. Spot the difference: MESP textured on van der Waals surface for $Si_{10}O_{10}H_{20}$. Actual and "synthesized" MESPs shown on the left and right sides, respectively. The ranges are in au.

Results and Discussion

The ab initio SCF calculations for the above molecules are carried out using the INDMOL program[15] on PARAM machine.[16] The basis sets chosen for the present work are STO-3G, 6-31G hondo, and 6-31G* for some cases. The error analysis is carried out for the tailored density matrices and gross features such as MESP on the van der Waals surface. Finer features as exemplified by the MESP critical points[8] (CPs) are also discussed along with MEF for some cases.

Some representative deviations in the tailored **P** from the actual one and the total SCF time required to obtain these matrices are presented in Table 1. For the systems discussed in Table 1, the calculation time of fragments is typically 10–15% of the actual ones. This advantage in SCF time grows with the enhancement in the basis set and the complexity of the molecule. The error analysis in Table 1 shows that the deviations of the synthesized **P** from the actual one are in the range of 10^{-3} au. For the above examples, the magnitudes of self- as well as near- (atom) neighbor **P** elements are all typically in the range ~0.5 to 2.5, becoming insignificant for the farther ones. Thus, the near- and farthest-neighbor interaction blocks in the actual density matrices are excellently simulated in the tailored ones. The patching zone is seen to be somewhat error prone. The maximum error (typically $\sim 10^{-2}$) in each test case has occurred in this region. As the major contributions are always from the self- and near-neighbor interactions, one may expect a good reproduction of molecular properties from the synthesized **P**. A test of goodness of the synthesized **P** is seen by evaluating trace(**PS**) (=number of electrons) and $\|\mathbf{PSP} - \mathbf{2P}\|$ ($=\max_{i,j}(|\mathbf{PSP} - \mathbf{2P}|)$ viz., idempotency test for **P**). For all the above test cases it has been seen that the trace(**PS**) gives to within 0.03% of the number of electrons for the corresponding system and $\|\mathbf{PSP} - \mathbf{2P}\|$ is at most 10^{-2}.

In the present work, MESP is employed for the appraisal of density matrices obtained from the tailoring approach. The differences in the "actual" and "synthesized" MESPs textured on van der Waals surfaces are indeed very difficult to be made out visually from Figure 3. It can be seen from Table 2 that the average absolute MESP value on the van der Waals surface for all the test cases is $\sim 10^{-2}$; whereas the standard and average deviations in the synthesized MESP from the actual one are in the range of 10^{-3}. These deviations are of the same order as that in the synthesized **P**. The maximum deviations are seen to have occurred in the patching zone. In general, the MESP obtained from the tailored density matrices on the van der Waals surface is in good agreement with that from the actual ones. Thus, gross features of MESP are well-simulated by the new method.

TABLE 2: Statistical Error Analysis for MESP Textured on van der Waals Surface Using Tailored Density Matrices and Exact Density Matrix (Values in au Wherever Appropriate)

molecule and basis set	no. of contraction	av[a] absolute MESP value	deviation[b]			total no. of points (N)
			std	av	max	
$Si_5O_{16}H_{12}$ (STO-3G)	137	2.67e–2	4.8e–3	3.1e–3	2.9e–2	33 854
$Si_{10}O_{10}H_{20}$ (STO-3G)	160	1.53e–2	5.0e–3	3.3e–4	2.6e–2	7 977

[a] Average absolute MESP value = $(1/N)\sum_{i=1}^{N}|V_i(\mathbf{r})|$. [b] Standard deviation = $\{(1/N)\sum_{i=1}^{n}(V(i)_{act} - V(i)_{syn})^2\}^{1/2}$. Average deviation = $(1/N)\sum_{i=1}^{N}|V(i)_{act} - V(i)_{syn}|$. V_{act} and V_{syn} stand for the actual and synthesized density matrices, respectively.

TABLE 3: Positions and Values of MESP Minima Corresponding to Oxygens in $Si_{10}O_{10}H_{20}$ (All Values in au)[a]

actual topography				"synthesized" topography			
x	y	z	$V(\mathbf{r})$	x	y	z	$V(\mathbf{r})$
24.967	–1.567	3.347	–0.1078	24.959	–1.561	3.340	–0.1088
23.247	0.396	1.587	–0.0992	23.241	0.377	1.579	–0.1008
15.448	1.908	2.836	–0.0902	15.450	1.904	2.833	–0.0904
19.628	1.798	0.175	–0.0716	19.627	1.798	0.175	–0.0719
13.412	–0.780	2.513	–0.0921	13.419	–0.792	2.511	–0.0928
12.947	–3.762	3.969	–0.0932	12.962	–3.765	3.954	–0.0941
13.727	–7.642	2.217	–0.0723	13.729	–7.640	2.217	–0.0729
18.047	–9.521	4.045	–0.0721	18.041	–9.537	4.109	–0.0730
21.658	–9.056	3.245	–0.0705	21.658	–9.053	3.271	–0.0710
24.080	–6.294	3.042	–0.0843	24.079	–6.292	3.037	–0.0846

[a] See text for further details.

To compare the *finer features* of the "actual" and "synthesized" MESP, the topographies of $Si_5O_{16}H_{12}$ (3G and 6-31G) and decamer rings have been studied. It is found that the position, nature, and the MESP values of the CPs are in good agreement with the actual ones in general.

In the case of $Si_5O_{16}H_{12}$, 10 minima are located using the actual **P**, of which those due to terminal oxygens are well mimiced with the concatenated **P** (with the maximum error of ~1% in MESP value and ~0.1 au in the positions). The maximum error is again seen to have occurred in the "joining" zone, comprising of oxygens connected to the central silicon. The positions of these minima are in good agreement with the original ones, although the MESP values are ~–0.05 au instead of ~–0.09 au. A reason for the errors which have occurred in the overlapping region for this test case is that, being a reasonably small molecule, it is not really well suited for fragmentation.

One of the real test cases for the appraisal of the tailoring scheme is offered by zeolite decamer ring systems. It is of great interest to observe the potential changes inside the decamer rings as these form the channels in the ZSM-5 zeolite. The topography of MESP inside the rings is therefore of relevance. Table 3 compares the positions and values of the minima inside the $Si_{10}O_{10}H_{20}$ ring. It can be observed from the Table 3 that the deviation in the positions and values of minima obtained from synthesized **P** are within 1% of the actual ones. It may be noted that our MESP minima are comparable to the typical ones reported by Brand et al.,[10] being in the range of –0.09 au for the STO-3G basis.

To judge whether the overlap achieved by the above fragmentation scheme for $Si_{10}O_{10}H_{20}$ is good enough, the system is studied using five $Si_4O_5H_{10}$ fragments. The O–Si–O–Si–O forms

TABLE 4: Synthesized Topography: Positions and Values of MESP Minima Corresponding to Oxygens in $Si_{10}O_{30}H_{20}$ (All Values in au)[a]

x	y	z	$V(\mathbf{r})$
24.936	−1.568	3.366	−0.1170
23.386	0.410	1.647	−0.1084
15.443	1.905	2.842	−0.1054
19.596	1.790	0.142	−0.0793
13.402	−0.780	2.555	−0.1016
12.945	−3.729	3.972	−0.1039
13.511	−7.792	1.988	−0.0880
18.034	−9.547	4.155	−0.0816
21.659	−9.043	3.237	−0.0843
24.072	−6.258	2.912	−0.0973

[a] See text for further details.

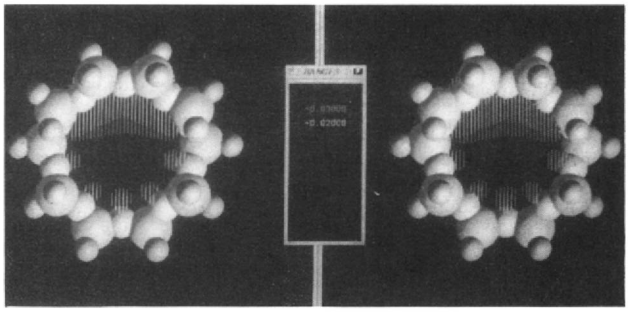

Figure 4. Spot the difference: MESP contours for decamer ring in silicalite. Actual and "synthesized" MESPs shown on the left and right sides, respectively. The ranges are in au.

the overlapping region as against O–Si–O in the earlier scheme, resulting into a better overlap. The results obtained are very similar to those reported above, proving that sufficient overlap is achieved with the earlier fragmentation scheme as well. The deviations in MESP are of the same order as those obtained for the above fragmentation scheme of one pentamer and two tetramers. It thus appears that a choice of O–Si–O as an overlapping fragment suffices to achieve realistic results.

Yet another example of this kind is that of the decamer $Si_{10}O_{30}H_{20}$ ring, without the substitution of the outer oxygens by hydrogens. The minima of $Si_{10}O_{30}H_{20}$ inside the ring turn out to be slightly deeper as compared to those in the $Si_{10}O_{10}H_{20}$ system (cf. Table 4). The goodness of the values and positions of the minima could not be tested due to the absence of the actual **P** for this system. However, extrapolating the decamer $Si_{10}O_{10}H_{20}$ ring results discussed above, one can reasonably trust these values and their positions inside the ring.

A particularly attractive test case of recent interest[14] rather similar to that discussed here is provided by another decamer ring system in silicalite. This system exhibits a large zone of negative MESP coupled with five small islands, engendering rather grossly anisotropic features. In this case, the system has been fragmented into five trimers (STO-3G basis set) with the overlap between two fragments being O–Si–O. As one can see from the Figure 4, the gross features of MESP are excellently reproduced. The negative MESP zone in the case of a synthesized molecule is slightly swollen. We also have an excellent reproduction of the negative MESP islands. The tailored density matrix, **P** for the decamer ring system in silicalite is also obtained for the 6-31G* basis set (380 contractions) using five tetramers. The MESP map for the system is similar in nature to that shown in Figure 4, though the MESP values are deeper at the minima.

Last, we test the proposed methodology for branched structures which are often encountered in biomolecules, as typified by a di- and tripeptide, viz., phe-his and phe-his-try. These cases consist of 40 and 64 atoms, respectively, and are spatially rather spreadout. The SCF calculations for both the above test cases are carried out with STO-3G basis (complete system and fragments) as well as 6-31G (only fragments) for the latter case. On the top side

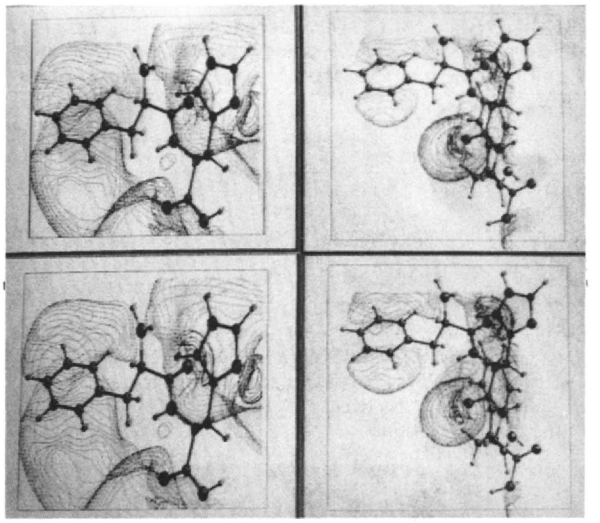

Figure 5. MESP contours for dipeptide (left) and tripeptide (right). SCF and tailored MESPs are at the top and bottom, respectively. The MESP contour values: dipeptide chain −0.005 and −0.08 au; tripeptide chain −0.01 and −0.08 au. See text for details.

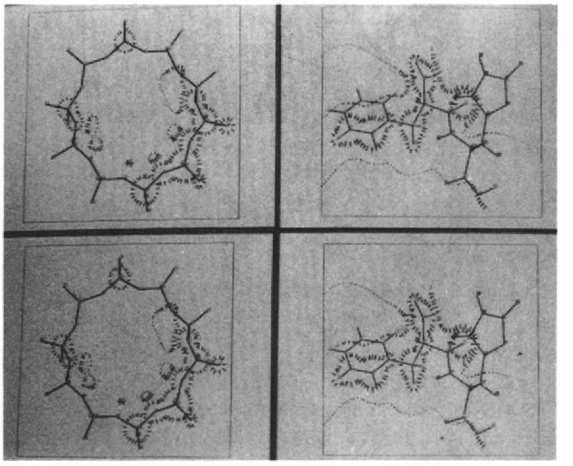

Figure 6. Maps of ∇V over a plane for a zeolite decamer ring (left) and dipeptide (right). SCF and tailored ∇V shown as the top and bottom parts respectively. See text for details.

of the Figure 5 are the MESP maps with actual density matrices and on the bottom are those with the synthesized ones. The di- and tripeptide systems appear on the left and right sides of the figure. One can readily notice from Figure 5 the excellent agreement of the MESPs with their actual counterparts. The "synthesized" MESP critical points also match quite well with the actual ones in position, value as well the nature. The maximum deviations in the positions and values of the CPs from the actual ones are observed to be less than 0.001 au. The MESP map, using synthesized **P**, for the tripeptide chain with 6-31G basis is qualitatively similar to that shown in Figure 5.

The electron density critical points obtained for both the peptides considered above using tailored density matrices also match with the same degree of accuracy as the MESP critical points when compared with their actual SCF counterparts.

For the examples considered above, it can be seen that the MESP distribution as well as the electron density and MESP critical points are very well reproduced. It is therefore intuitively expected that the MEF is also reproduced well. To illustrate this fact we consider MEF for two examples, viz., the decamer ring $Si_{10}O_{10}H_{20}$ system and dipeptide system. The MEF for both these cases is evaluated over a set of planes using actual ab initio SCF **P** and the synthesized **P**. The "synthesized" MEF in both the cases considered above match to within 1% of the actual one (cf. Figure 6). The left part of Figure 6 shows the negative of MEF (viz. ∇V) map over an arbitrary plane for the decamer ring.

The arrows in the figure show the direction of ∇V and are suitably scaled. The field using synthesized **P** (bottom left) shows almost no difference when compared with its actual (top left) counterpart. On the right side of Figure 6 we have the MEF for dipeptide evaluated over an arbitrary plane. The figure shows that the "synthesized" ∇V (bottom right) is well-reproduced for the dipeptide system when compared with the actual one (top right).

Concluding Remarks

The current work presents a novel and simple way of simulating electrostatics of large molecules by stitching together the respective smaller fragment counterparts. The **P** thus tailored does indeed mimic global features of electrostatics of large systems. The "stitching scheme" provides in a way a *divide and conquer* strategy. One divides a given system into smaller fragments with a care to keep sufficient overlaps among them and carries out their SCF computations independently. For large systems, the total computation time for all the fragments added together is *much smaller* as compared to that for the parent system (as also earlier noted by Lee and Friesner[13]). Thus, for very large molecules, the fragmentation approach is expected to be immensely beneficial as one may be unable to get the actual ab initio SCF **P** within reasonable time span with the available hardware. As in the present work, density matrices for the systems $Si_{10}O_{30}H_{20}$ (3G, 260 contractions), decamer ring in silicalite (6-31G*, 380 contractions) and tripeptide chain (6-31G, 380 contractions) have been synthesized with the tailoring approach even though the actual ones could not be obtained. The SCF for the fragments has been carried out on a larger configuration of PARAM[16] with 64 nodes, an i860 and BFS. The total calculation time in the former case is 7686 s, whereas in the latter cases it is about 50 000 s. Thus, even with small computers, one is not deprived of working on larger molecular systems.

To check how the synthesized **P** fares in the actual SCF iterations, these matrices for the above test cases are supplied as initial guesses to the respective SCF computations and the first iteration energy compared with the final converged one. It has been seen that the uniterated energy obtained from the synthesized **P** agrees to within 1% of the final converged energy. The difference is even less (~0.01%) for large systems. This brings home the goodness of tailored density matrices.

The current work demonstrates that MESP as well as MEF of the synthesized molecule closely resembles the actual one. Thus, it is expected that the assembled density matrices will also be able to well simulate other one-electron properties such as the density, dipole moment, etc. With the encouraging results on MESP topography, one can use these "stitched" matrices for obtaining the point charges for very large systems: their performance is expected to be at least as good as that reported by Lee and Friesner,[13] since no *P2zero*- and *P3zero*-type assumptions are invoked by us.

It is expected that our new method will be a boon for those having access to only PC-level and workstation-range machines. One can thus hope to simulate features of ab initio MESP with extremely good accuracy without taking recourse to less reliable and sometimes heavily parametrized semiempirical methods. Further, the time advantage is expected to significantly enhance with the size of the molecule for supercomputer environments as well. Our approach thus hopefully represents "art of the possible" for studying molecular electrostatics of large systems.

Acknowledgment. The authors are grateful to the Center for Development of Advanced Computing (C-DAC), Pune, and Council of Scientific and Industrial Research (CSIR), New Delhi, for support. Thanks are due to Dr. R. Vetrivel, Professors A. C. Hess, and A. S. Kolaskar for supplying us with the molecular geometries employed in this work. We thank the referees for useful suggestions.

References and Notes

(1) Pullman, B. *Int. J. Quantum Chem. Quantum Biol. Symp.* **1990**, *17*, 81.

(2) Politzer, P., Truhlar, D. G., Eds. *Chemical Applications of Atomic and Molecular Electrostatic Potential*; Plenum: New York, 1981.

(3) Tomasi, J.; Bonaccorsi, R.; Cammi, R. In *Theoretical Models of Chemical Bonding*; Maksic, R., Ed.; Springer: Berlin, 1990; pp 230–268.

(4) Scrocco, E.; Tomasi, J. *Adv. Quantum Chem.* **1978**, *11*, 116.

(5) Sjoberg, P.; Politzer, P. *J. Phys. Chem.* **1989**, *94*, 3425.

(6) Pathak, R. K.; Gadre, S. R. *J. Chem. Phys.* **1990**, *93*, 17. Gadre, S. R.; Pathak, R. K. *Proc. Indian Acad. Sci. (Chem. Sci.)* **1990**, *18*, 102.

(7) Gadre, S. R.; Kulkarni, S. A.; Shrivastava, I. H. *J. Chem. Phys.* **1992**, *96*, 5253. Gadre, S. R.; Shrivastava, I. H. *J. Chem. Phys.* **1991**, *94*, 8384.

(8) Shirsat, R. N.; Bapat, S. V.; Gadre, S. R. *Chem. Phys. Lett.* **1992**, *200*, 373. The critical point (CP) of a scalar field f is a point where $\nabla f = 0$. All three eigenvalues of the Hessian matrix at the CP are positive for a (3,+3) minimum. A (3,–1) saddle corresponds to two negative and one positive eigenvalue. For details, see: Bader, R. F. W. *Atoms in Molecules, a quantum theory*; Clarendon Press: Oxford, 1990, and references therein.

(9) Kollman, P.; Rothenberg, S. *J. Am. Chem. Soc.* **1977**, *99*, 1333. Ghio, C.; Tomasi, J. *Theor. Chim. Acta (Berlin)* **1973**, *30*, 151.

(10) Brand, H. V.; Curtiss, L. A.; Iton, L. E. *J. Phys. Chem.* **1993**, *97*, 12773.

(11) Naray-Szabo, G. *Int. J. Quantum Chem.* **1979**, *16*, 265. Naray-Szabo, G.; Grofcsik, A.; Kasa, K.; Kubinyi, K.; Martin, A. *J. Comput. Chem.* **1981**, *2*, 58. Lavery, R.; Pullman, A.; Wen, Y. *Int. J. Quantum Chem.* **1983**, *24*, 353. Nagy, P.; Ángyán, J. G.; Naray-Szabo, G.; Peirel, G. *Int. J. Quantum Chem.* **1987**, *31*, 927.

(12) Spangler, D.; Christoffersen, R. E. In *Adv. Quantum Chem.* **1972**, *6*, 333.

(13) Lee, J. G.; Friesner, R. A. *J. Phys. Chem.* **1993**, *97*, 3515.

(14) White, J. C.; Hess, A. C. *J. Phys. Chem.* **1993**, *97*, 8703.

(15) Shirsat, R. N.; Limaye, A. C.; Gadre, S. R. *J. Comput. Chem.* **1993**, *14*, 445.

(16) Eknath, P. R.; L. Bhasin, L.; Degwekar, A. In *Advanced Computing*; Bhatkar, V. P., Ed.; Tata McGraw-Hill: Delhi, 1991, p 86.